

Informative Sample Mining Network for Multi-Domain Image-to-Image Translation

Jie Cao, Huaibo Huang, Yi Li, Ran He, Zhenan Sun

CRIPAC & NLPR, Institute of Automation, Chinese Academy of Sciences
University of Chinese Academy of Sciences

{jie.cao, huaibo.huang, yi.li}@cripac.ia.ac.cn, {rhe, znsun}@nlpr.ia.ac.cn

Abstract

The performance of multi-domain image-to-image translation has been significantly improved by recent progress in deep generative models. Existing approaches can use a unified model to achieve translations between all the visual domains. However, their outcomes are far from satisfying when there are large domain variations. In this paper, we reveal that improving the strategy of sample selection is an effective solution. To select informative samples, we dynamically estimate sample importance during the training of Generative Adversarial Networks, presenting Informative Sample Mining Network. We theoretically analyze the relationship between the sample importance and the prediction of the global optimal discriminator. Then a practical importance estimation function based on general discriminators is derived. In addition, we propose a novel multi-stage sample training scheme to reduce sample hardness while preserving sample informativeness. Extensive experiments on a wide range of specific image-to-image translation tasks are conducted, and the results demonstrate our superiority over current state-of-the-art methods.

1. Introduction

Multi-domain image-to-image translation (I2I) aims at learning the mappings between visual domains. These domains can be instantiated by a set of attributes, each of which represents a meaningful visual property. Since each possible combination of the attributes specifies a unique visual domain [24], the total domain number can be very large in practical applications. For instance, if there are 10 independent binary attributes, we need to handle the translations among 1024 visual domains, which is far more challenging than two-domain translation. Fortunately, thanks to the advances in deep generative models [5, 15], current methods [1, 8, 18, 31] are able to achieve multi-domain I2I by

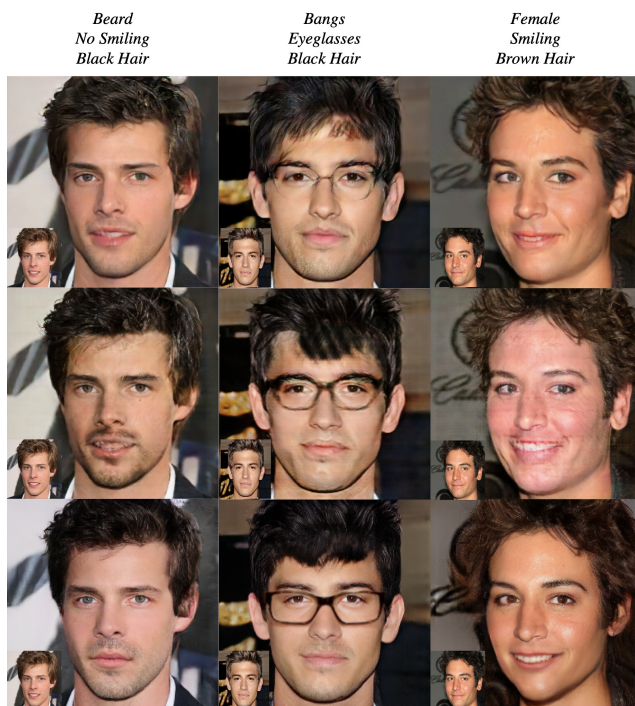


Figure 1: Facial attribute transfer results of different methods (top: AttGAN [8], middle: STGAN [18], bottom: ours). For each column, the inputs are transformed according to the attributes specified on the top of the images. We place each input at the bottom left corner of the corresponding result. While AttGAN and STGAN show degraded results in these challenging cases, our method achieves effective attribute transfer and maintains the realism of texture details.

a single model. However, these methods mainly produce promising results when translating images within similar visual domains, *e.g.*, changing different hair colors of human. The translations between domains with large semantic discrepancy are still not well addressed yet.

To further illustrate the limitation of existing approaches, we take the task of facial attribute transfer as a prime example. Fig. 1 shows the results of some challenging translations. Due to the large gap between the source and the target domain, it is difficult to transfer attributes without impairing visual realism. Even the current state-of-the-art methods [8, 18] produce degraded results, although they can address most of the easy translations (we will show them in following experiments). This phenomenon indicates that existing methods mainly focus on solving the easy cases during training but neglect the hard ones.

We argue that effective sample selection strategies greatly help to address this problem. Sample selection is within the scope of deep metric learning, which contributes to many computer vision tasks. The studies in deep metric learning [11, 25, 33, 35] point out that a large fraction of training samples may satisfy the loss constraints, providing no progress for model learning. That is, the vast majority of samples are too easy and their contributions to training are only marginal. Unfortunately, current multi-domain I2I methods merely adopt the naive random sample selection that treats all training samples equally and thus selects easy ones mostly. It intuitively hinders training efficiency and consequently leads to the degradation discussed above.

In this paper, we propose **Informative sample mining network (INIT)** to enhance training efficiency and improve performance in multi-domain I2I tasks. Concretely, we integrate Importance Sampling into the generation framework under Generative Adversarial Networks (GAN). Adversarial Importance Weighting is proposed to select informative samples and assign them greater weight. We derive the weighting function based on the assumption that the global optimal discriminator is known. Then we consider more general conditions and introduce the guidance from the prior model to rescale the importance weight. Furthermore, we propose Multi-hop Sample Training to avoid the informative samples from becoming too hard to train, which is a longstanding problem [25, 30, 35]. Based on the principle of divide-and-conquer, we produce target images by multiple hops, which means the image translation is decomposed into several separated steps. On the one hand, our training scheme preserves the informativeness of the samples. On the other hand, learning translations step-by-step effectively reduces the hardness of samples. Equipped with Adversarial Importance Weighting and Multi-hop Sample Training, our approach can probe and then fully utilize informative training samples.

To verify the effectiveness of our approach, we conduct experiments on facial attribute transfer, season transfer, and sketch&photo transfer. We make extensive comparisons with current state-of-the-art multi-domain I2I methods. The experimental results demonstrate our improvements in both attribute transfer and content preserving.

Our contributions can be summarized as follows:

- We analyze the importance of sample selection in image-to-image translation and propose Informative Sample Mining Network.
- We propose Adversarial Importance Weighting which integrates Importance Sampling into GAN, to achieve effective training sample mining.
- We propose Multi-hop Sample Training to reduce the hardness of the probed informative samples, making them easy to train.
- We provide extensive experimental results on facial attribute transfer, season transfer, and sketch&photo transfer, showing our superiority over existing approaches.

2. Related work

Image-to-Image Translation. Recent advances in deep generative models [5, 15, 22] have brought much progress in image-to-image translation [1, 8, 12, 16, 18, 19, 31, 36]. At the early stage, the studies are focused on translations between two visual domains. Zhu *et al.* make pioneering works on learning the translations with paired data [12] and unpaired data [36]. FaderNet [16] disentangles the salient information in the latent space to control attribute intensity. UNIT [19] combines Variational AutoEncoder [15] with GAN, and present high-quality results on unsupervised translation tasks. Later on, a lot of efforts are made to deal with the multi-domain condition. StarGAN [1] is the first unified model that produces visually plausible multi-domain translation results. AttGAN [8] introduces an attribute-aware constraint as well as a reconstruction-based regularization to achieve “only change what you want”. Following AttGAN, Liu *et al.* [18] propose a novel selective transfer unit to enhance image quality. RelGAN [31] introduces the notion of relative attribute and employs multiple discriminators to improve both attribute translation and interpolation. Different from previous approaches, we make improvements from a new perspective: we probe informative samples during training, making our network aware of the most challenging cases.

Deep Metric Learning. Deep metric learning aims at learning good representations. The core idea is to narrow the distances of similar images in the embedding space and enlarge the distances of dissimilar ones. Existing works mainly focus on how to choose proper loss functions and sample selection strategies. In the studies of loss function, contrastive loss [10] and triplet loss [28] are the most representative works. The two loss functions are widely adopted and extended by successive methods. Huang *et al.* [11] explore the structure of quadruplets. Wang *et al.* [29] improve

triplet loss by introducing a third-order geometry relationship. Sample selection strategies have also been widely studied. For example, hard negative sample mining [26] is proposed to replace the random sample selection in the contrastive loss. FaceNet [25] first adopts semi-hard negative mining within a batch for face recognition. Harwood *et al.* [6] utilize approximate nearest neighbor search to select harder samples adaptively. Recently proposed methods [2, 34] introduce adversarial learning to generate potentially informative samples to train the model. At present, sample selection strategies have been adopted in many computer vision tasks, including image recognition [17], face verification [10, 25], and person re-identification [32]. In this work, we argue that sample strategy is also important to image generation but rarely studied. To this end, we propose a novel sampling strategy specifically for multi-domain I2I.

Importance Sampling. In statistics, Importance Sampling [4] is a method for estimating properties of a target distribution $p_{data}(\mathbf{x})$ which is difficult to sample from directly. Samples are instead drawn from a proposal distribution $p_g(\mathbf{x})$, which is easier to sample from. Assume that for any point \mathbf{x} in the sample space, we have $p_g(\mathbf{x}) > 0$ whenever $p_g(\mathbf{x}) \cdot p_{data}(\mathbf{x}) \neq 0$. Then, we can draw samples from $p_g(\mathbf{x})$ to estimate $\mathbb{E}_{p_{data}}[\mathcal{L}(\mathbf{X})]$ for any known function \mathcal{L} . Specifically, we have

$$\begin{aligned} \mathbb{E}_{p_{data}}[\mathcal{L}(\mathbf{X})] &= \int \frac{p_{data}(\mathbf{x})}{p_g(\mathbf{x})} \mathcal{L}(\mathbf{x}) p_g(\mathbf{x}) d\mathbf{x} \\ &= \mathbb{E}_{p_g} \left[\frac{p_{data}(\mathbf{X})}{p_g(\mathbf{X})} \mathcal{L}(\mathbf{X}) \right], \end{aligned} \quad (1)$$

where the likelihood ratio $\frac{p_{data}(\mathbf{x})}{p_g(\mathbf{x})}$ is denoted as the importance weight. In this paper, we introduce Importance Sampling into GAN. Hence, $p_g(\mathbf{x})$, $p_{data}(\mathbf{x})$ and \mathcal{L} denote the generator distribution, the true data distribution, and the adversarial loss function, respectively. In Section 3.1, we will describe how to calculate the importance weight under the GAN framework.

3. Proposed Method

We consider visual domains characterized by an n -dimensional binary attribute vector $\mathbf{a} = [a_1, a_2, \dots, a_n]^T$, where each bit a_i represents a meaningful visual attribute. We build Informative Sample Mining Network to learn all the mappings between these domains from unpaired training data. Our network takes a source image \mathbf{x}^s with a target attribute \mathbf{a}^t , and produces a fake target image \mathbf{x}^t . In the following part, we will introduce Adversarial Importance Weighting (AIW) in Section 3.1, Multi-hop Sample Training (MST) in Section 3.2, and the implementation details in Section 3.3.

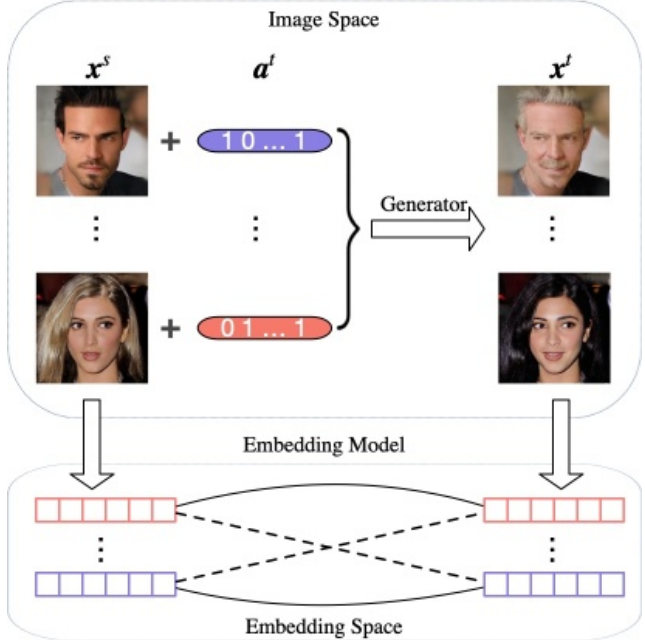


Figure 2: A visual illustration about how we select inter-class and intra-class pairs. The solid lines in the embedding space connect intra-class pairs, and the dash lines connect inter-class pairs. Within each batch, we calculate the mean distances of the two kinds of pairs.

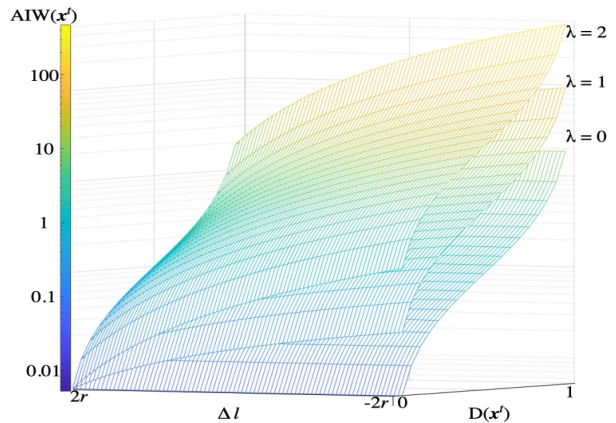


Figure 3: A visualization of AIW function with different λ . By adjusting the hyperparameter λ , we can make our sample weight estimation more radical or more conservative.

3.1. Adversarial Importance Weighting

We adopt a GAN-based network as our backbone model. That is, we train the generator and make the generator distribution p_g to capture the true data distribution p_{data} . Meanwhile, a discriminator tries to distinguish the real data from the fake data synthesized by the generator. The generator and the discriminator are trained jointly by optimizing the

adversarial loss, which can be written as:

$$\min_G \max_D \mathcal{L} = \mathbb{E}_{\mathbf{x}^s, \mathbf{a}^s \sim p_{data}} [\log D(\mathbf{x}^s, \mathbf{a}^s)] + \mathbb{E}_{\mathbf{x}^t, \mathbf{a}^t \sim p_g} [\log (1 - D(\mathbf{x}^t, \mathbf{a}^t))], \quad (2)$$

where $\mathbf{x}^t = G(\mathbf{x}^s, \mathbf{a}^t)$. For brevity, We use G and D to denote the generator and the discriminator, respectively. The inputs of G and D are the concatenation of an image and an attribute vector. Note that we apply spatial replication on the attribute vector, making the sizes of the image and the attribute vector matched.

By optimizing the formulated adversarial loss, we can make G learn how to translate images into any target domain specified by \mathbf{a}^t . However, Eq. 2 simply adopts the random sample selection, whose limitations have been discussed in Section 1. In this section, we make improvements by introducing Importance Sampling into our model. To this end, we need to determine the importance weight, *i.e.*, $\frac{p_{data}(\mathbf{x})}{p_g(\mathbf{x})}$ in Eq. 1. Recall the proposition made in GAN [5]: for any fixed G and any sample point \mathbf{x} , we have

$$D^*(\mathbf{x}) = \frac{p_{data}(\mathbf{x})}{p_{data}(\mathbf{x}) + p_g(\mathbf{x})}, \quad (3)$$

where D^* is the global optimal discriminator. In our task, the notation of \mathbf{x} should be replaced by \mathbf{x}^t . Then, let $D(\mathbf{x}) = \frac{1}{e^{-\tilde{D}(\mathbf{x})} + 1}$, and we have

$$D^*(\mathbf{x}^t) = \frac{1}{1 + e^{-\tilde{D}^*(\mathbf{x}^t)}} = \frac{p_{data}(\mathbf{x}^t)}{p_{data}(\mathbf{x}^t) + p_g(\mathbf{x}^t)}, \quad (4)$$

$$\frac{p_{data}(\mathbf{x}^t)}{p_g(\mathbf{x}^t)} = e^{\tilde{D}^*(\mathbf{x}^t)}.$$

For any fake target sample \mathbf{x}^t , we can determine its importance weight by Eq. 4. A greater $\tilde{D}^*(\mathbf{x}^t)$ brings \mathbf{x}^t a bigger weight, which means \mathbf{x}^t is more informative. In the meantime, a greater $\tilde{D}^*(\mathbf{x}^t)$ leads to a greater $D^*(\mathbf{x}^t)$, which means \mathbf{x}^t is harder to distinguish. We can see that similar to existing sample selection strategies, **mining the informative samples in GAN means finding the hard samples**.

In practice, we cannot get the optimal discriminator. D may not provide accurate weight estimation if our model is too far away from the global optimality. Hence, we need to measure how close our network is to the optimal condition. In this section, we propose a heuristic metric that calculates sample distances in the embedding space. To this end, we first project samples onto a hypersphere whose radius is r by a pre-trained embedding model. Then, we calculate the inter-class point distance l_n and intra-class l_p point distance. Note that the distance in the embedding space reflects the semantic distance between data points, so l_n should be as

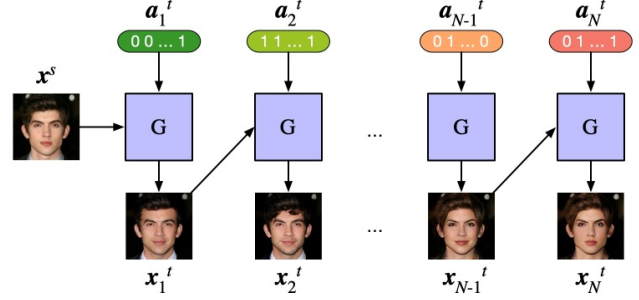


Figure 4: An illustration about N-hop sample generation. After N times of translations, the generator produces the N-hop target image \mathbf{x}_N^t . $\mathbf{x}_1^t, \mathbf{x}_2^t, \dots, \mathbf{x}_{N-1}^t$ are intermediate images.

large as possible, and l_p should be as small as possible. In the optimal situation, $l_n^* = 2r$, $l_p^* = 0$. In practical conditions, we can compute $\Delta l = l_n - l_p$ and use $(\Delta l^* - \Delta l)$ to estimate how close our network is to the global optimality. Concretely, we use $(\Delta l^* - \Delta l)$ to rescale the importance weight, proposing Adversarial Importance Weighting:

$$\text{AIW}(\mathbf{x}^t) = [1 + (\Delta l^* - \Delta l)]^\lambda \cdot e^{\tilde{D}(\mathbf{x}^t)}, \quad (5)$$

where λ is a hyperparameter. In our experiment, we calculate Δl in a batch-wise manner. Within each batch, we compute the mean distances of inter-class and intra-class pairs as l_n and l_p , respectively. As illustrated in Fig. 2, for each source image, its corresponding target image has the same content information, so the two images compose an intra-class pair in the embedding space. Similarly, the other pairs in the batch are considered as inter-class pairs, since the content information is different.

Our AIW has following properties:

- 1) $\Delta l^* = \Delta l = 2r$ is the optimal condition. In this case, sample weights assigned by AIW equal to $e^{\tilde{D}(\mathbf{x}^t)}$.
- 2) In practical conditions, we have $0 < \Delta l^* - \Delta l \leq 4r$. A bigger $(\Delta l^* - \Delta l)$ indicates larger difference from the optimal condition, and therefore AIW makes more significant modifications on $e^{\tilde{D}(\mathbf{x}^t)}$ in this case.
- 3) λ controls the dynamic range of AIW. A larger λ means AIW is more radical and tends to assign greater weights to informative samples.

To further illustrate these properties, we visualize the surfaces of AIW function with different λ in Fig. 3. As indicated by Property 1, when $\Delta l = 2r$, all the surfaces intersect at the same line: $\text{AIW}(\mathbf{x}^t) = e^{\tilde{D}(\mathbf{x}^t)}$. The color in the figure indicates weight value, and a larger λ makes informative samples have greater weights.

3.2. Multi-hop Sample Training

AIW can effectively probe hard informative samples for model training. However, the studies [25, 30, 35] in metric learning reveal that mining too hard samples may lead to severe training problems, especially when training data is noisy. Hence, many efforts [2, 6, 25, 35] have been made to seek semi-hard samples to address this issue. In this section, we introduce Multi-hop Sample Training for the same purpose but in a new perspective: instead of sidestepping the hardest samples, we reduce sample hardness in a divide-and-conquer manner.

In I2I, we use the word ‘‘hop’’ to denote the translation time a model takes to produce the target result. Fig. 4 provides a visual illustration, and below we give a formal definition:

$$\mathbf{x}_N^t = \overbrace{G(\dots G(G(\mathbf{x}^s, \mathbf{a}_1^t), \mathbf{a}_2^t), \dots), \mathbf{a}_N^t)}^N, \quad (6)$$

where \mathbf{x}_N^t denotes N-hop target image. \mathbf{x}_N^t is transformed by the generator N times, and turns into the target image at the last time. The attribute of \mathbf{x}_N^t is only determined by \mathbf{a}_N^t . The intermediate attributes $\mathbf{a}_1^t, \mathbf{a}_2^t, \dots, \mathbf{a}_{N-1}^t$, which determines the attributes of intermediate images, can be randomly chosen.

Previous approaches mainly utilize 1-hop target image during training. In contrast, N-hop Sample Training considers {1-hop, 2-hop, ..., N-hop} target images. When $n = 2, \dots, N$, we randomly draw m groups of intermediate attributes for each n . In our experiments, we set $m = 5$. We also generate 1-hop target image, which does not have any intermediate image. Given a training pair $(\mathbf{x}^s, \mathbf{a}^t)$, we first draw the intermediate attributes and produce the multiple hop target images. Then, we calculate losses on all the target and intermediate images. In this manner, the translation from the source domain to the target domain is broken down into multiple separated steps. Our loss function provides supervision information for each step. Hence, MST effectively reduces the hardness of training samples.

3.3. Implementation Details

We can now propose the complete training algorithm of our model, which combines AIW and MST. We first produce 1-hop target images, just as previous approaches. Then, we estimate the importance weight of fake samples by the 1-hop images. Next, we draw intermediate attributes and produces multi-hop target images. Finally, we update model parameters by optimizing the weighted adversarial loss calculated on the multi-hop results. Note that multi-hop target and intermediate images have the same weights as the corresponding 1-hop images. Following the classical GAN [5], we optimize G and D iteratively. The training process is summarized in Algorithm 1.

Algorithm 1: Training algorithm of INIT

-
- 1 Pretrain the embedding model ϕ
 - 2 Initialize the generator G and the discriminator D
 - 3 **for** the number of training epochs **do**
 - 4 Sample $\{(\mathbf{x}^{s1}, \mathbf{a}^{t1}), (\mathbf{x}^{s2}, \mathbf{a}^{t2}), \dots, (\mathbf{x}^{sn}, \mathbf{a}^{tn})\}$
 - 5 G forward propagates, producing 1-hop images
 - 6 D forward propagates
 - 7 Use AIW to calculate sample weights by 1-hop images
 - 8 Draw intermediate attributes
 - 9 G forward propagates, producing multi-hop results
 - 10 D forward propagates
 - 11 Calculate the weighted form of the adversarial loss \mathcal{L} in Eq. 2 on multi-hop results
 - 12 Optimize G by minimizing \mathcal{L}
 - 13 Optimize D by maximizing \mathcal{L}
 - 14 **end**
-

Metric	StarGAN [1]	AttGAN [8]	STGAN [18]	Ours
FID	19.28	13.62	15.94	11.16
Mean Acc	90.03	93.56	92.98	95.08

(a) The comparisons of FID and Mean ACC.

Attribute	StarGAN [1]	AttGAN [8]	STGAN [18]	Ours	Real Data
Hair Color	91.02	93.10	92.45	94.47	96.12
Aging	92.38	95.41	95.22	97.90	98.42
Bangs	87.97	91.03	91.84	93.26	93.67
Smile	85.53	90.47	87.41	90.94	91.00
Gender	90.72	96.77	94.76	96.57	98.25
Beard	87.90	93.53	93.09	95.58	95.34
Skin Color	89.35	92.65	94.03	94.69	94.22
Eyeglasses	93.38	96.44	96.09	98.46	99.31

(b) The comparisons of the ACC of each class.

Table 1: The comparisons of Fréchet Inception Distance [9] (FID, lower is better) and the classification accuracy [31] (ACC, higher is better) on facial attribute transfer.

In our experiments, we empirically set $\lambda = 2$ in AIW and adopt 2-hop MST. We build a fully convolutional network as our generator and use a patch discriminator similar to [36]. The pre-trained VGG [27] is employed as the embedding model. Specifically, we use VGGFace [23] for facial attribute transfer. Please see our supplementary for more details about the network architecture. We optimize model parameters by Adam optimizer [14] with $\beta_1 = 0.5$, $\beta_2 = 0.999$, and a learning rate of $1e-4$.

4. Experiments

To validate the effectiveness of our approach, we perform extensive experiments on facial attribute transfer, season transfer, and sketch&photo transfer. We produce 256 × 256 results and train our model as well as other compet-

ing models for 100 epochs. Our batch size is set to 16. In the following part, we first describe the datasets in our experiments (Section 4.1). Then we make comparisons with existing methods and report experimental results (Section 4.2, 4.3, and 4.4). Finally, we present an ablation study (Section 4.5). Besides, please refer to our supplementary for more visual examples.

4.1. Dataset

CelebA [20] is the largest publicly available dataset for multi-domain I2I tasks at present. There are annotations of 40 binary attributes for each image. In our experiment, we use the high-quality version, CelebA-HQ [13], for facial attribute transfer. We choose the following 10 attributes to construct the attribute vector: *Black_Hair*, *Blond_Hair*, *Brown_Hair*, *Bangs*, *Smiling*, *Male*, *No_Beard*, *Pale_Skin*, and *Eyeglasses*. We randomly select 300 images as the testing set and use all the remaining images for training.

Yosemite Flickr Dataset [36] consists of 1,200 winter photos and 1,540 summer photos of Yosemite National Park. It is widely used for season transfer, which is an unpaired I2I problem. In our experiment, we follow the training and testing data divisions of CycleGAN [36].

Sketch2Photo Dataset [3] contains photos of 250 categories of objects and the corresponding sketches. Pix2pix [12] first uses the shoes category for sketch-to-photo transfer. We follow the training and testing data divisions in Pix2pix to train our model.

4.2. Facial Attribute Transfer

We compare with StarGAN¹ [1], AttGAN² [8], and STGAN³ [18] on facial attribute transfer. We reproduce their results by the released source codes. The training and testing data for all the compared methods are the same.

Fig. 5 shows single attribute transfer results. Given an input image, each method produces 10 transformed images. For each output result, one specific attribute is toggled. For relatively easy tasks like changing hair color, all the methods produce plausible results. By contrast, when dealing with the challenging ones like aging, our method produces more realistic results. In general, our INIT can achieve effective attribute transfer and outperform other methods.

We argue that **multiple attribute transfer** should also be emphasized. Transferring multiple attributes is at least no easier than transferring single one, and the number of possible combinations is significantly larger. Hence, the hard cases are mainly from the multiple attribute conditions. We report comparison results of multiple facial attribute transfer in Fig. 1 and Fig. 6. In these cases, keeping visual quality and achieving effective attribute transfer become far more

Metric	CycleGAN [36]	StarGAN [1]	STGAN [18]	Ours
FID	48.40/49.39	44.84/52.16	45.61/50.37	40.09/44.91
Votes	3.73	11.07	21.52	63.68

(a) The comparison results of season transfer.

Metric	Pix2pix [12]	StarGAN [1]	AttGAN [8]	Ours
FID	39.59/17.13	33.23/13.92	29.01/13.86	28.44/12.30
Votes	30.26	3.77	6.44	59.53

(b) The comparison results of sketch&photo transfer.

Table 2: The comparisons of FID and user votes (percentage). For season transfer, the FID is reported as “summer/winter”. For sketch&photo transfer, the FID is reported as “photo/sketch”.

challenging. However, our INIT can still produce desired results. Thanks to the weighting strategies, our method pays more attention to the hard cases and therefore yields a better performance. Our superiority provides a strong evidence on the effectiveness of sample selection.

We also calculate Fréchet Inception Distance (FID) [9] and the classification accuracy [31] to make objective comparisons. Lower FID is better, since it means that the Wasserstein distance between the real distribution and the generated distribution is smaller. The classification accuracy reflects the effectiveness of attribute transfer, and thus higher is better. Following [18], we train a Resnet-18 [7] as the classifier and calculate the accuracy on the transformed results. To train this classifier, we use the same data division of CelebA-HQ [13] as the division for our generation tasks. In Table 1a, we summarize FID and the mean classification accuracy. Furthermore, we report the accuracy of each class in Table 1b. It can be observed that our method has the best performance, indicating our improvements in visual realism and attribute transfer.

4.3. Season Transfer

For season transfer, we make comparisons with CycleGAN [36], StarGAN [1], and STGAN [18]. Note that only CycleGAN trains a pair of networks to achieve *summer*→*winter* and *winter*→*summer*, respectively. The other approaches can achieve season transfer by a single model.

We summarize the visual examples of translation results in Fig. 7. We also calculate FID as an objective metric. Since real summer and winter photos have apparent perceptual discrepancy, we calculate FID on the two seasons separately. Furthermore, we conduct a user study. We invite volunteers to select the best result among the transformed images from the four methods. All the testing images are compared, and we report voting percentages of different methods. The quantitative comparison results are summarized in Table 2a. The comparison on FID indicates that

¹<https://github.com/yunjey/stargan>

²<https://github.com/elvisyjlin/AttGAN-PyTorch>

³<https://github.com/bluestyle97/STGAN-pytorch>



Figure 5: Visual examples of single facial attribute editing results. From top to down, the rows are results of StarGAN [1], AttGAN [8], STGAN [18], and our INIT.

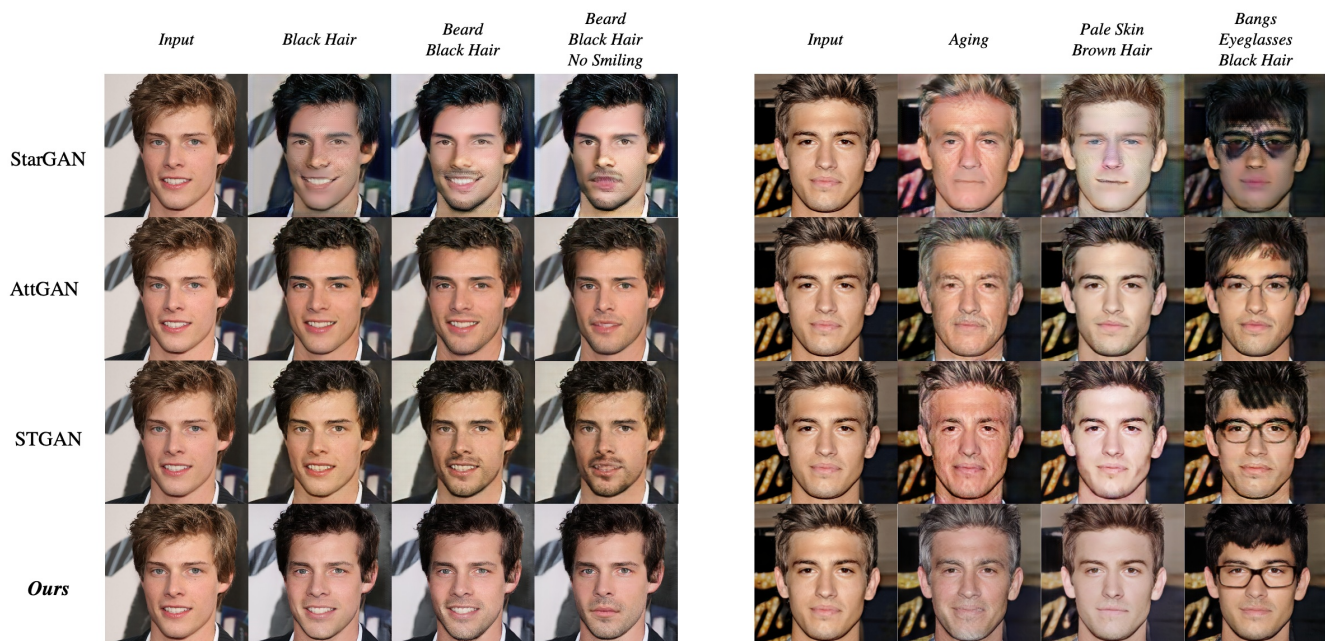


Figure 6: Visual examples of multiple facial attribute editing, which is a very challenging case in multi-domain I2I. We make comparisons with StarGAN [1], AttGAN [8], STGAN [18].

our approach favorably outperforms the competing methods, and we obtain the majority of the user votes.

4.4. Sketch&Photo Transfer

In this subsection, our method is compared with Pix2pix [12], StarGAN [1], and AttGAN [8] on sketch&photo transfer. Pix2pix needs to learn sketch-to-photo and photo-to-sketch separately, and the other methods can deal with the two translations simultaneously. Since we have paired data in this dataset, we add the L1 distance

loss [12] in the pixel space, which is useful for paired I2I tasks. Note that we also add the L1 loss for the other competing methods to make fair comparisons.

We report the examples of translation results and the ground truth in Fig. 8. Similar to season transfer, we calculate FID and conduct user study, the results of which are reported in Table 2b. Learning sketch-to-photo and photo-to-sketch as two separated tasks brings Pix2pix obvious advantages, but our method still has the best performance. Compared with StarGAN and AttGAN, our method pro-

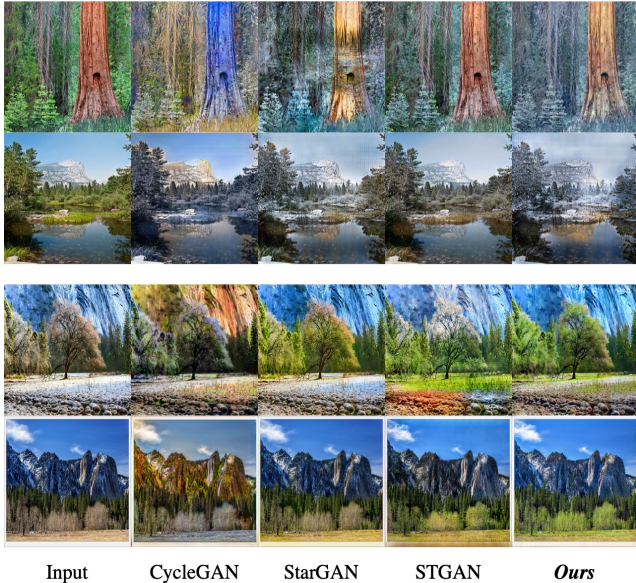


Figure 7: Visual examples of season translation. We compare with CycleGAN [36], StarGAN [1], and STGAN [18]. The top two rows are *summer*→*winter*, and the bottom two rows are *winter*→*summer*.



Figure 8: Visual examples of sketch&photo transfer. We compare with Pix2pix [12], StarGAN [1], and AttGAN [8]. The top two rows are *sketch*→*shoes*, and the bottom two rows are *shoes*→*sketch*. The ground truths are placed on the upper left corners of the inputs.

duces more plausible results, showing stronger generalization ability for paired I2I tasks.

Model	AIW	Hop Number	FID	Mean Acc
(a)	<i>w/o</i>	2	18.91	92.86
(b)	<i>w/</i>	3	11.23	94.98
(c)	<i>w/</i>	2	11.16	95.08
(d)	<i>w/</i>	1	14.52	93.78
(e)	<i>w/o</i>	1	21.38	91.44

Table 3: Comparison results of different variations of our method. Our full model is equivalent variation (c).

4.5. Ablation Study

In this subsection, we conduct ablation study to verify the effectiveness of AIW and MST. To this end, we implement several variations of our approach and evaluate them on facial attribute transfer. Concretely, we consider the following variations: a) INIT without any importance sampling schemes, b-d) INIT with n -hop sample training, where $n = 3, 2, 1$, respectively. e) INIT without AIW and MST, *i.e.*, simply a conditional GAN [21]. Note that our full model, INIT, is equivalent variation (c).

We use the same experiment setting and train these variations for the same number of iterations. Note that variations with a smaller hop number will have more iterations for training new samples, since they have fewer intermediate results to optimize. Tabel 3 shows comparison results on quantitative metrics, and please refer to our supplementary for visual examples. Through ablation study, we can verify the following two points:

Mining informative samples plays an important role.

Without the important sampling scheme, the performances of variations (a) and (e) drop sharply. Even when we double the training iterations of variation (e), its performance is still obviously inferior. Hence, merely taking more training time is not an effective option in multi-domain I2I. By comparing variations (c) and (e), we can see that AIW contributes the most to our improvements. These results verify the importance of our proposed AIW, which achieves effective sample weighting.

The optimal choice is 2-hop sample training.

Among the variations with different hops, variation (c) has the best performance. This observation verifies the effectiveness of multi-hop sample training. Another interesting finding is that more hops do not further improve the performance. We think that 2-hop sample training achieves the balance between mining more samples and reducing the hardness of existing samples.

5. Conclusion

In this paper, we propose to integrate Importance Sampling into a GAN-based model, resulting in Adversarial Importance Weighting for high-quality multi-domain image-to-image translation. Furthermore, Multi-hop Sam-

ple Training subtly reduces sample hardness while preserving sample informativeness. Thanks to the improvements in training efficiency, our approach achieves effective translation even when dealing with a large number of challenging visual domains. We conduct extensive experiments on practical tasks, including facial attribute transfer, season transfer, and sketch&photo transfer. The results consistently demonstrate our superiority to existing methods.

References

- [1] Yunjey Choi, Minje Choi, Munyoung Kim, Jung-Woo Ha, Sunghun Kim, and Jaegul Choo. StarGAN: Unified generative adversarial networks for multi-domain image-to-image translation. In *CVPR*, 2018.
- [2] Yueqi Duan, Wenzhao Zheng, Xudong Lin, Jiwen Lu, and Jie Zhou. Deep adversarial metric learning. In *CVPR*, 2018.
- [3] Mathias Eitz, James Hays, and Marc Alexa. How do humans sketch objects? In *SIGGRAPH*, 2012.
- [4] Michael Evans, Tim Swartz, et al. Methods for approximating integrals in statistics with special emphasis on bayesian integration problems. *Stat Sci*, 1995.
- [5] Ian Goodfellow, Jean Pouget-Abadie, Mehdi Mirza, Bing Xu, David Warde-Farley, Sherjil Ozair, Aaron Courville, and Yoshua Bengio. Generative adversarial nets. In *NeurIPS*, 2014.
- [6] Ben Harwood, BG Kumar, Gustavo Carneiro, Ian Reid, Tom Drummond, et al. Smart mining for deep metric learning. In *ICCV*, 2017.
- [7] Kaiming He, Xiangyu Zhang, Shaoqing Ren, and Jian Sun. Deep residual learning for image recognition. In *CVPR*, 2016.
- [8] Zhenliang He, Wangmeng Zuo, Meina Kan, Shiguang Shan, and Xilin Chen. AttGAN: Facial attribute editing by only changing what you want. *TIP*, 2019.
- [9] Martin Heusel, Hubert Ramsauer, Thomas Unterthiner, Bernhard Nessler, Günter Klambauer, and Sepp Hochreiter. GANs trained by a two time-scale update rule converge to a Nash equilibrium. In *NeurIPS*, 2017.
- [10] Junlin Hu, Jiwen Lu, and Yap-Peng Tan. Discriminative deep metric learning for face verification in the wild. In *CVPR*, 2014.
- [11] Chen Huang, Chen Change Loy, and Xiaoou Tang. Local similarity-aware deep feature embedding. In *NeurIPS*, 2016.
- [12] Phillip Isola, Jun-Yan Zhu, Tinghui Zhou, and Alexei A Efros. Image-to-image translation with conditional adversarial networks. In *CVPR*, 2017.
- [13] Tero Karras, Timo Aila, Samuli Laine, and Jaakko Lehtinen. Progressive growing of GANs for improved quality, stability, and variation. In *ICLR*, 2018.
- [14] Diederik P Kingma and Jimmy Ba. Adam: A method for stochastic optimization. In *ICLR*, 2015.
- [15] Diederik P Kingma and Max Welling. Auto-encoding variational bayes. In *ICLR*, 2014.
- [16] Guillaume Lample, Neil Zeghidour, Nicolas Usunier, Antoine Bordes, Ludovic Denoyer, and Marc’Aurelio Ranzato. Fader networks: Manipulating images by sliding attributes. In *NeurIPS*, 2017.
- [17] Marc T Law, Nicolas Thome, and Matthieu Cord. Quadruplet-wise image similarity learning. In *ICCV*, 2013.
- [18] Ming Liu, Yukang Ding, Min Xia, Xiao Liu, Errui Ding, Wangmeng Zuo, and Shilei Wen. STGAN: A unified selective transfer network for arbitrary image attribute editing. In *CVPR*, 2019.
- [19] Ming-Yu Liu, Thomas Breuel, and Jan Kautz. Unsupervised image-to-image translation networks. In *NeurIPS*, 2017.
- [20] Ziwei Liu, Ping Luo, Xiaogang Wang, and Xiaoou Tang. Deep learning face attributes in the wild. In *ICCV*, 2015.
- [21] Mehdi Mirza and Simon Osindero. Conditional generative adversarial nets. *arXiv preprint arXiv:1411.1784*, 2014.
- [22] Aaron van den Oord, Nal Kalchbrenner, and Koray Kavukcuoglu. Pixel recurrent neural networks. In *ICML*, 2016.
- [23] Omkar M Parkhi, Andrea Vedaldi, Andrew Zisserman, et al. Deep face recognition. In *BMVC*, 2015.
- [24] Vishal M Patel, Raghuraman Gopalan, Ruonan Li, and Rama Chellappa. Visual domain adaptation: A survey of recent advances. *Signal Process. Mag.*, 2015.
- [25] Florian Schroff, Dmitry Kalenichenko, and James Philbin. Facenet: A unified embedding for face recognition and clustering. In *CVPR*, 2015.
- [26] Edgar Simo-Serra, Eduard Trulls, Luis Ferraz, Iasonas Kokkinos, Pascal Fua, and Francesc Moreno-Noguer. Discriminative learning of deep convolutional feature point descriptors. In *ICCV*, 2015.
- [27] Karen Simonyan and Andrew Zisserman. Very deep convolutional networks for large-scale image recognition. *arXiv preprint arXiv:1409.1556*, 2014.
- [28] Jiang Wang, Yang Song, Thomas Leung, Chuck Rosenberg, Jingbin Wang, James Philbin, Bo Chen, and Ying Wu. Learning fine-grained image similarity with deep ranking. In *CVPR*, 2014.
- [29] Jian Wang, Feng Zhou, Shilei Wen, Xiao Liu, and Yuanqing Lin. Deep metric learning with angular loss. In *ICCV*, 2017.
- [30] Chao-Yuan Wu, R Manmatha, Alexander J Smola, and Philipp Krahenbuhl. Sampling matters in deep embedding learning. In *ICCV*, 2017.
- [31] Po-Wei Wu, Yu-Jing Lin, Che-Han Chang, Edward Y Chang, and Shih-Wei Liao. RelGAN: Multi-domain image-to-image translation via relative attributes. In *ICCV*, 2019.
- [32] Rui Yu, Zhiyong Dou, Song Bai, Zhaoxiang Zhang, Yongchao Xu, and Xiang Bai. Hard-aware point-to-set deep metric for person re-identification. In *ECCV*, 2018.
- [33] Yuhui Yuan, Kuiyuan Yang, and Chao Zhang. Hard-aware deeply cascaded embedding. In *ICCV*, 2017.
- [34] Yiru Zhao, Zhongming Jin, Guo-jun Qi, Hongtao Lu, and Xian-sheng Hua. An adversarial approach to hard triplet generation. In *ECCV*, 2018.
- [35] Wenzhao Zheng, Zhaodong Chen, Jiwen Lu, and Jie Zhou. Hardness-aware deep metric learning. In *CVPR*, 2019.
- [36] Jun-Yan Zhu, Taesung Park, Phillip Isola, and Alexei A Efros. Unpaired image-to-image translation using cycle-consistent adversarial networks. In *ICCV*, 2017.

Informative Sample Mining Network for Multi-Domain Image-to-Image Translation Supplementary Material

1. Network Architecture

In this work, we implement our method based on Pytorch. In our experiments, the batch size is 16 and the image size is $[3 \times 256 \times 256]$. Given a n -dimensional attribute vector, we apply spatial replication to change its shape to $[n \times 256 \times 256]$. The inputs of the generator and the discriminator are both the concatenations of images and attribute vectors. Hence, the input tensor shape is $[(3 + n) \times 256 \times 256]$. The network architectures of the discriminator and the generator are reported in Table 1 and Table 2, respectively.

2. Additional Results

We report additional visual comparisons in this section. Please note that **we have downsampled the images in our supplementary to avoid oversized submission**. The single facial attribute transfer results are shown in Figures 1 and 2. The multiple facial attribute transfer results are shown in Figures 3, 4, and 5. For multiple facial attribute transfer, we also visualize the residual heatmaps between the inputs and the outputs to reveal the modified regions of images. We report more season transfer results in Figure 6 and more sketch&photo transfer results in Figure 7. Furthermore, we report the visual comparisons of our variations in the ablation study in Figure 8. Figures 9 and 10 show our results on facial attribute interpolation. We can control the intensity of the transferred attribute by interpolating the attribute vector.

These additional visual results further demonstrate the superiority of our approach. The results of other methods are not satisfying in some specific challenging cases, although they can also address most of the easy cases. For instance, STGAN always produces unrealistic facial skin when altering *age*. AttGAN tends to make modifications minor than expected when altering *gender* or *beard*. In general, our approach produces most plausible results with finer texture details.

Layer Type	Output Shape	Parameter Number
Conv2d	[64,128,128]	3,136
InstanceNorm2d	[64,128,128]	128
LeakyReLU	[64,128,128]	0
Conv2d	[128,64,64]	151,680
InstanceNorm2d	[128,64,64]	256
LeakyReLU	[128,64,64]	0
Conv2d	[256,32,32]	524,544
InstanceNorm2d	[256,32,32]	512
LeakyReLU	[256,32,32]	0
Conv2d	[512,16,16]	2,097,664
InstanceNorm2d	[512,16,16]	1,024
LeakyReLU	[512,16,16]	0
Conv2d	[1,16,16]	513

Table 1. The network architecture of our discriminator.

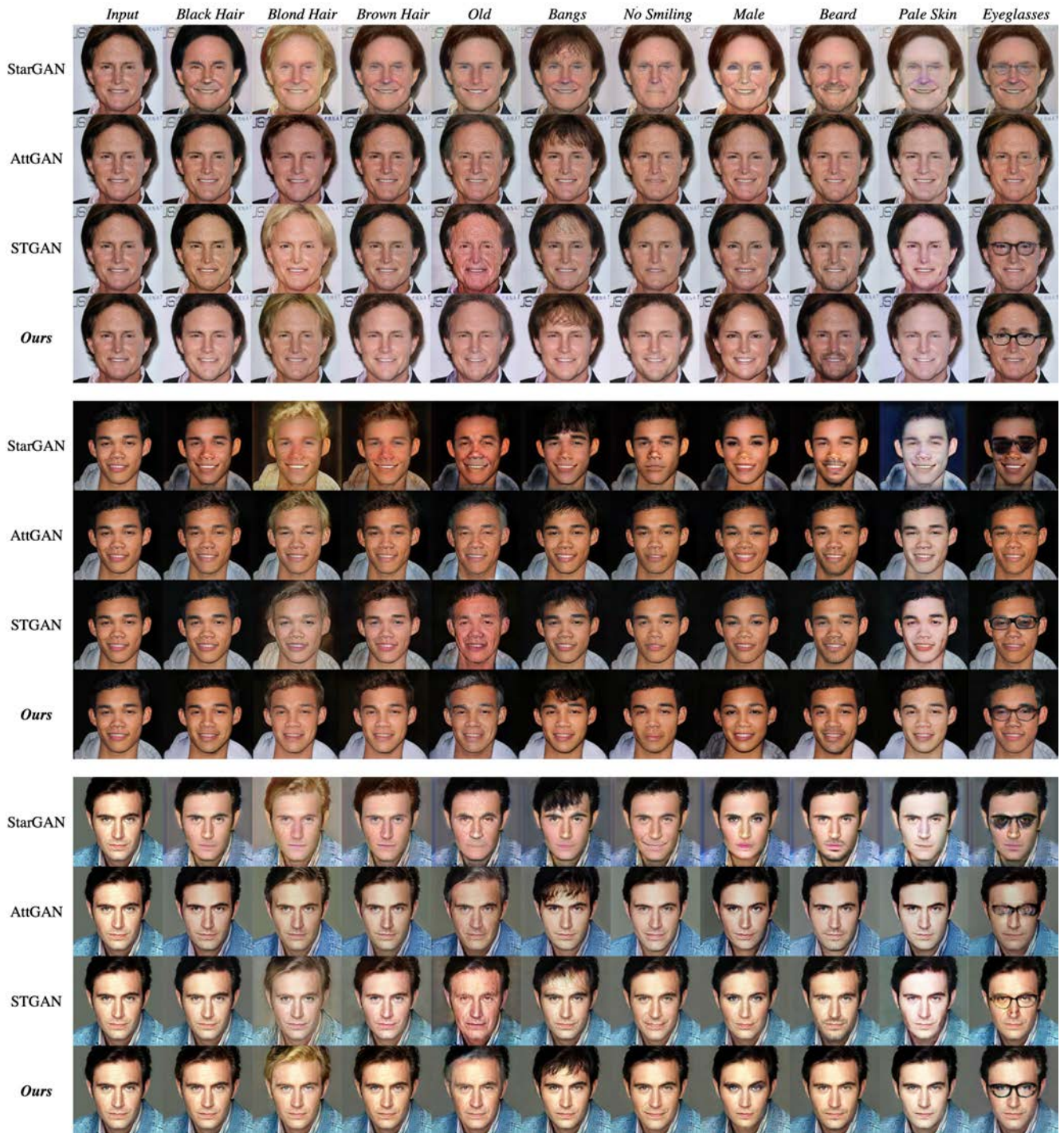


Figure 1. Visual examples of single facial attribute editing results. From top to bottom, the rows are results of StarGAN, AttGAN, STGAN, and our INIT.

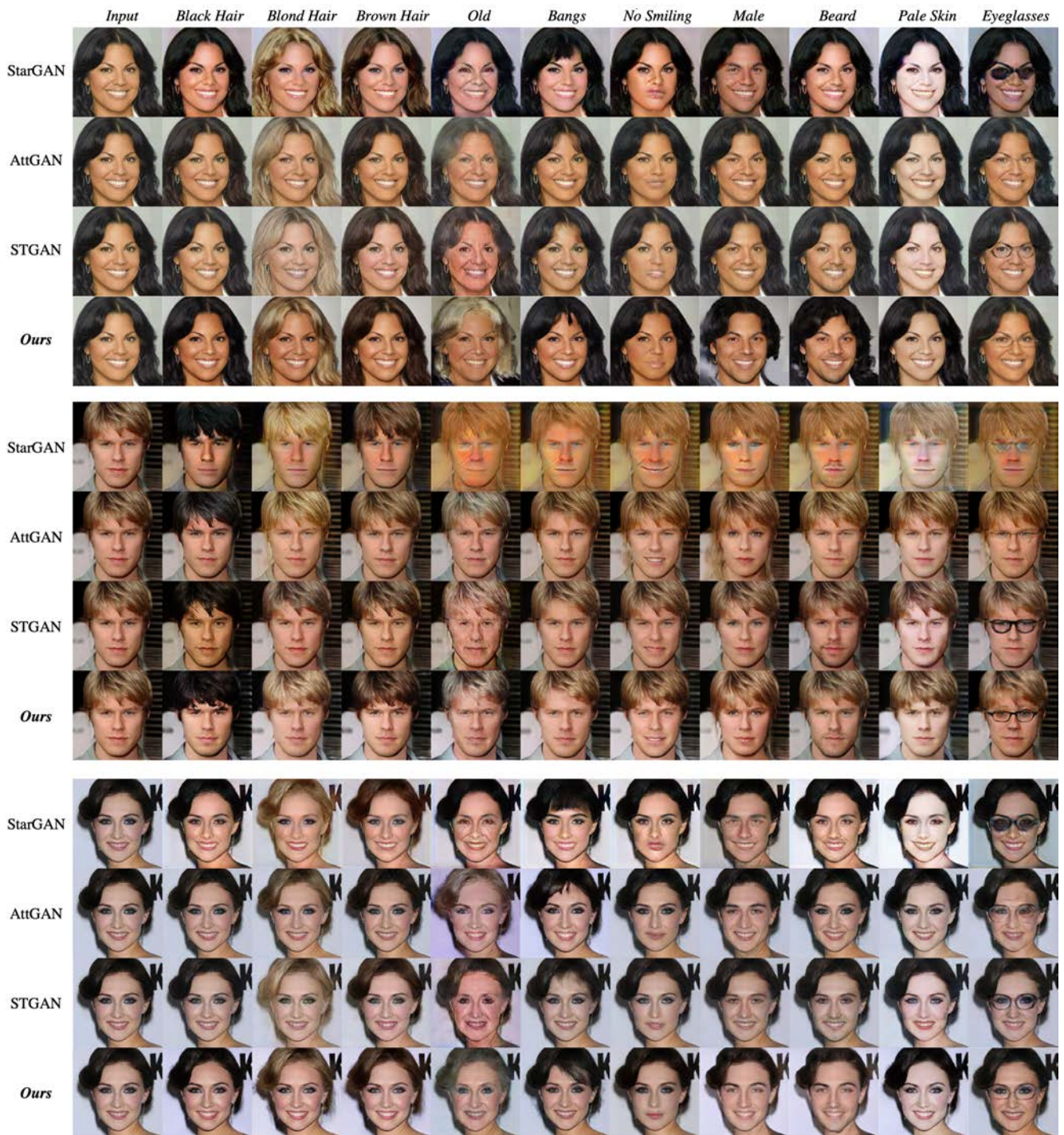


Figure 2. Visual examples of single facial attribute editing results. From top to bottom, the rows are results of StarGAN, AttGAN, STGAN, and our INIT.

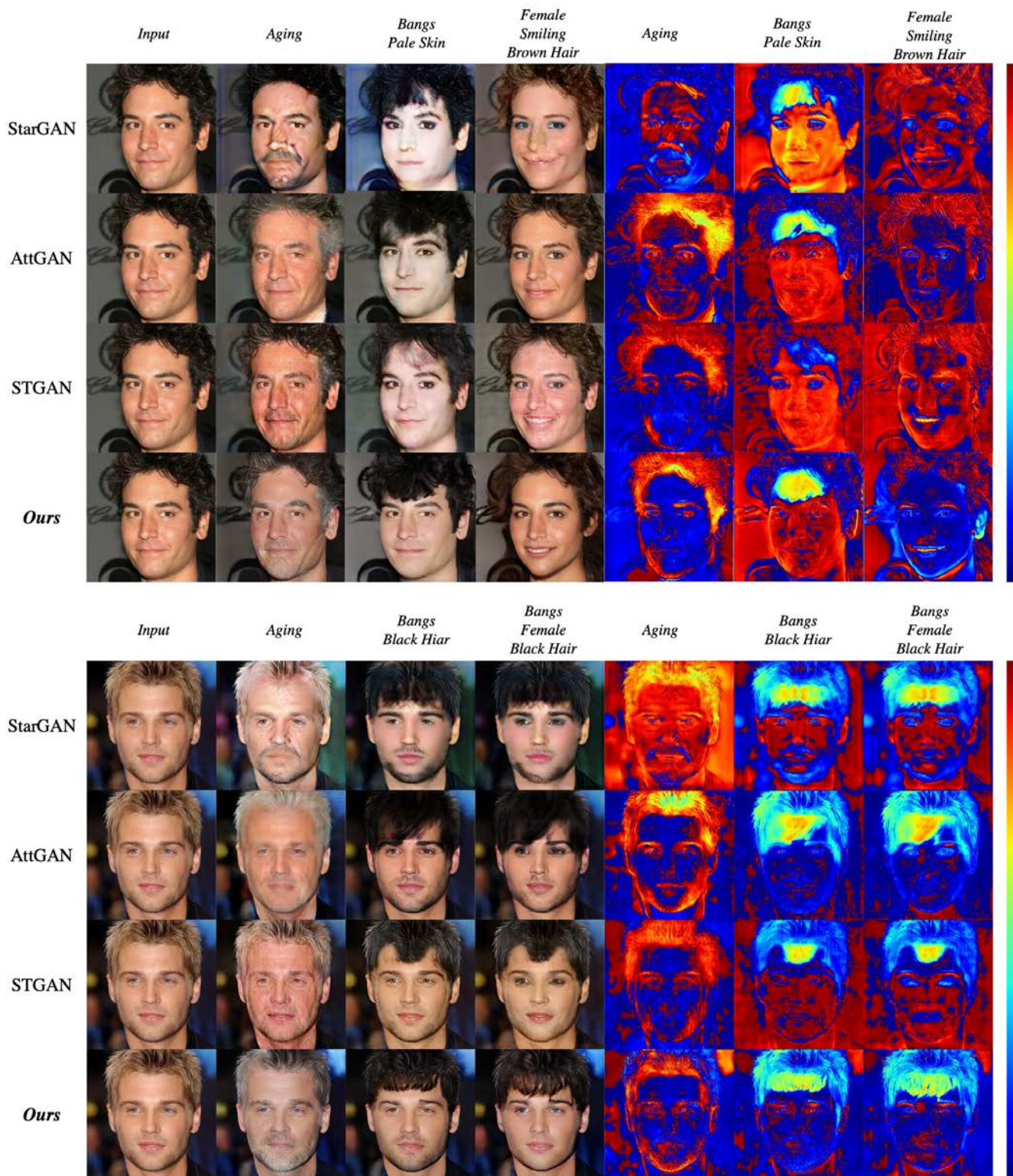


Figure 3. Visual examples of multiple facial attribute editing results. The residual heat maps visualize the differences between the inputs and the outputs. Please zoom in for better visualization.

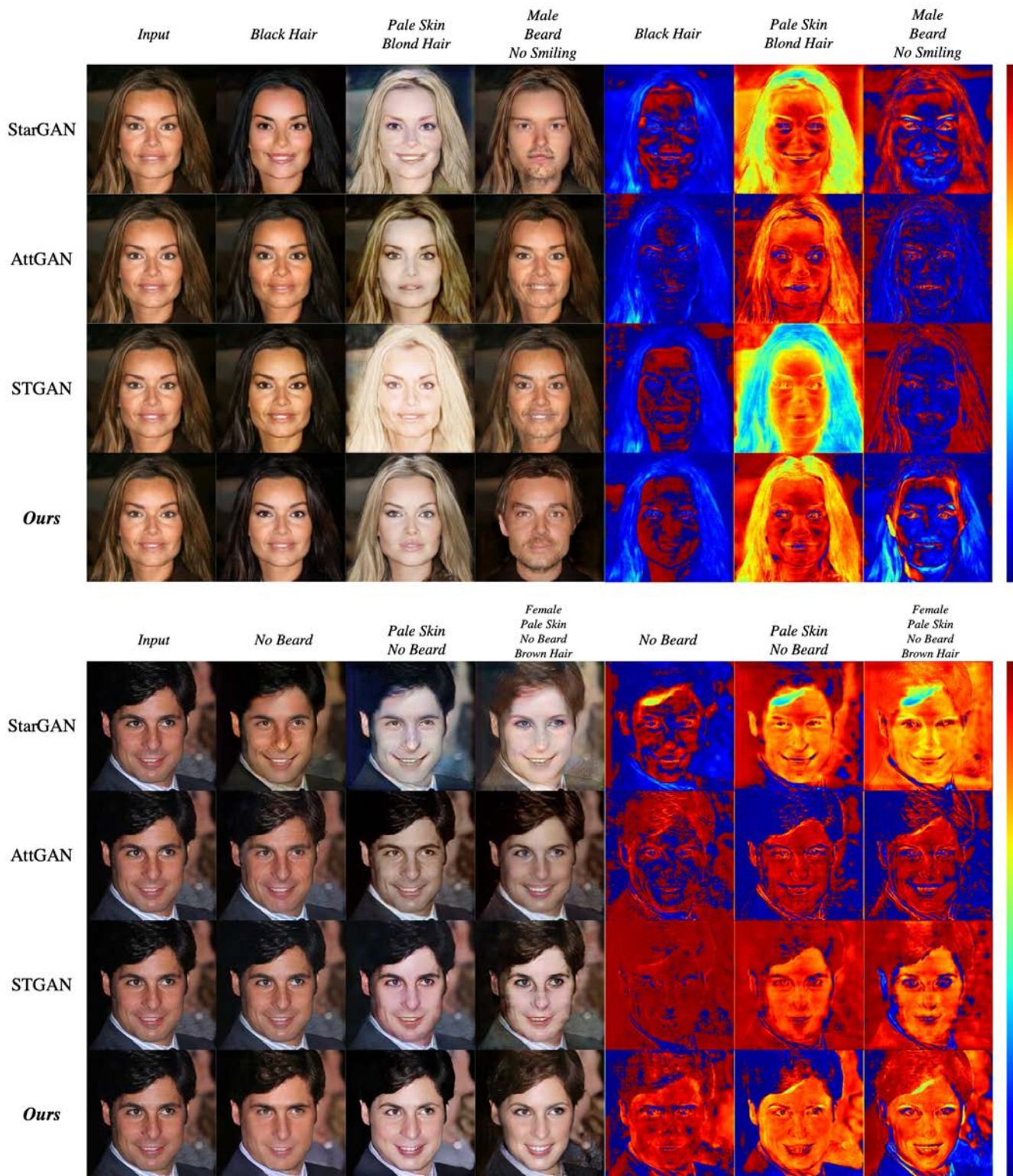


Figure 4. Visual examples of multiple facial attribute editing results. The residual heat maps visualize the differences between the inputs and the outputs. Please zoom in for better visualization.

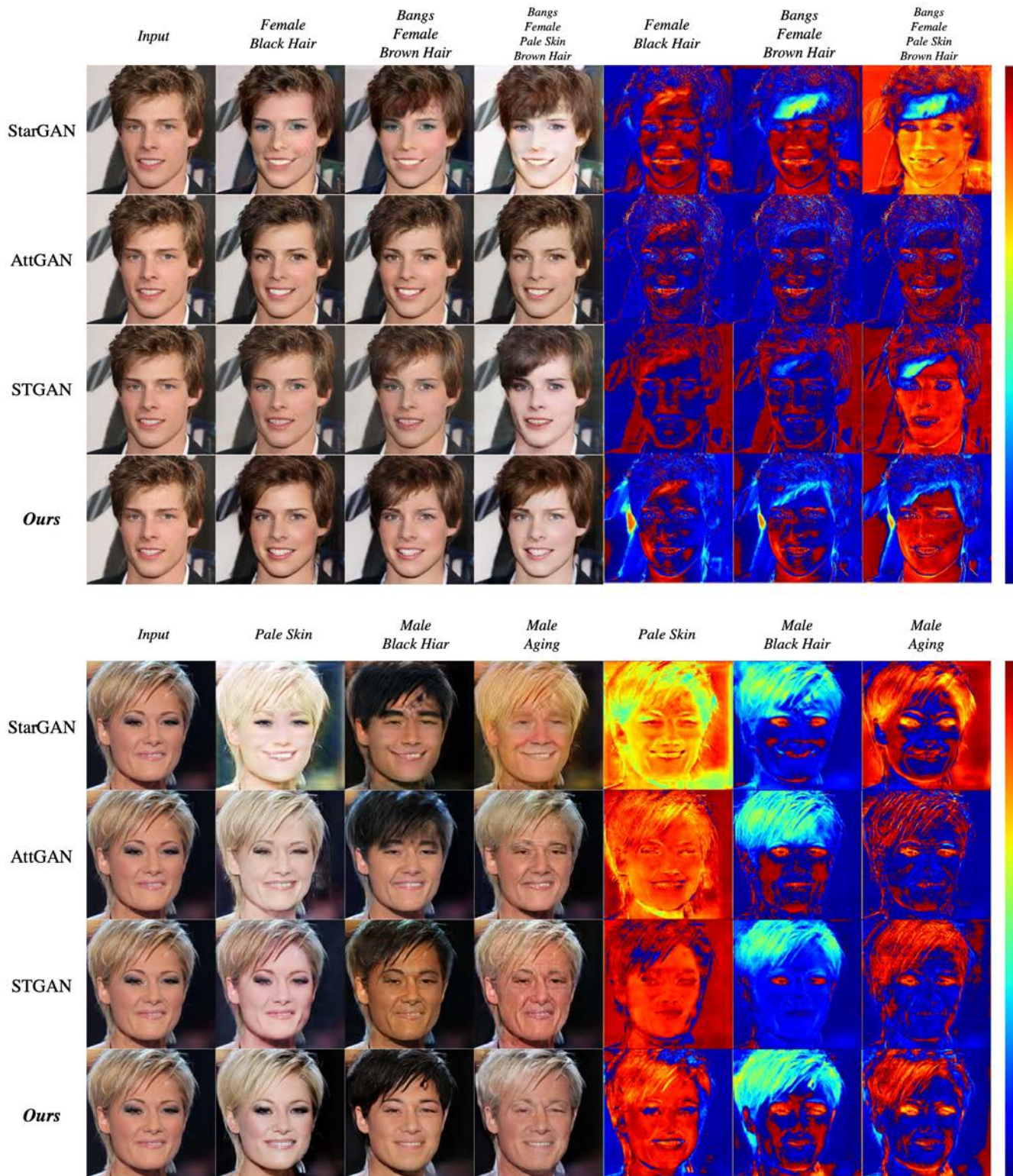


Figure 5. Visual examples of multiple facial attribute editing results. The residual heat maps visualize the differences between the inputs and the outputs. Please zoom in for better visualization.

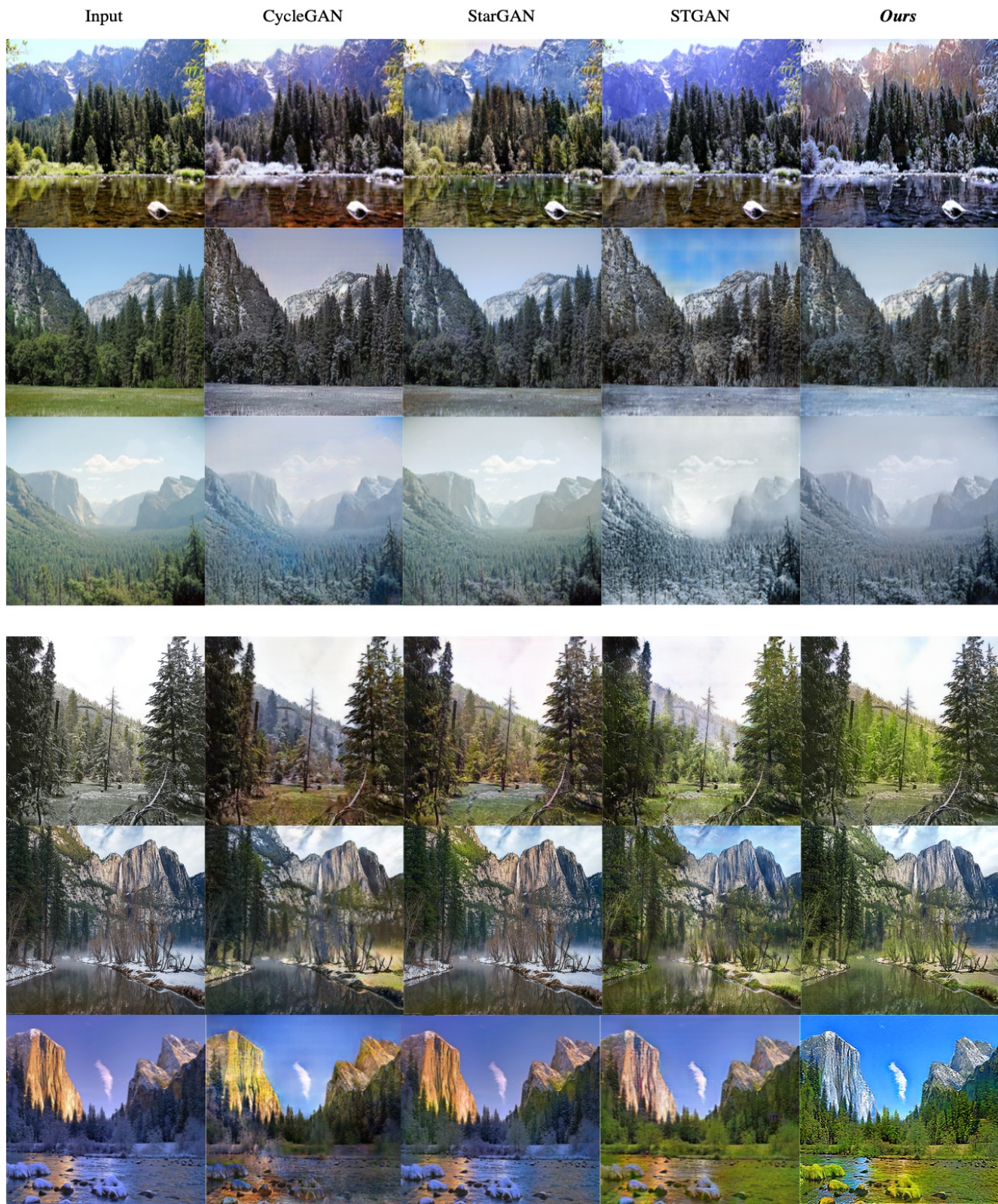


Figure 6. Visual examples of season translation. The top three rows are *summer*→*winter*, and the bottom three rows are *winter*→*summer*.



Figure 7. Visual examples of sketch&photo transfer. The top three rows are *sketch*→*shoes*, and the bottom three rows are *shoes*→*sketch*. The ground truths are placed on the upper left corners of the inputs.



Figure 8. Facial attribute transfer result comparisons of our variations in ablation study. For each row, the input is placed on the low left corner of the output of variation (a). Our full model is equivalent variation (c).



Figure 9. Facial attribute interpolation results. Our INIT can control the intensity of the transferred attribute by varying α . The interpolated attribute is *hair color*.



Figure 10. Facial attribute interpolation results. Our INIT can control the intensity of the transferred attribute by varying α . From top to bottom, the interpolated attributes are *smiling*, *pale skin*, *male*, *beard*, and *eyeglasses*.

Layer Type	Output Shape	Parameter Number
Conv2d	[64,256,256]	40,832
InstanceNorm2d	[64,256,256]	128
ReLU	[64,256,256]	0
Conv2d	[128,128,128]	131,200
InstanceNorm2d	[128,128,128]	256
ReLU	[128,128,128]	0
Conv2d	[256,64,64]	524,544
InstanceNorm2d	[256,64,64]	512
ReLU	[256,64,64]	0
Conv2d	[256,64,64]	590,080
InstanceNorm2d	[256,64,64]	512
ReLU	[256,64,64]	0
Conv2d	[256,64,64]	590,080
InstanceNorm2d	[256,64,64]	512
Conv2d	[256,64,64]	590,080
InstanceNorm2d	[256,64,64]	512
ReLU	[256,64,64]	0
Conv2d	[256,64,64]	590,080
InstanceNorm2d	[256,64,64]	512
Conv2d	[256,64,64]	590,080
InstanceNorm2d	[256,64,64]	512
ReLU	[256,64,64]	0
Conv2d	[256,64,64]	590,080
InstanceNorm2d	[256,64,64]	512
Conv2d	[256,64,64]	590,080
InstanceNorm2d	[256,64,64]	512
ReLU	[256,64,64]	0
Conv2d	[256,64,64]	590,080
InstanceNorm2d	[256,64,64]	512
Conv2d	[256,64,64]	590,080
InstanceNorm2d	[256,64,64]	512
ReLU	[256,64,64]	0
Conv2d	[256,64,64]	590,080
InstanceNorm2d	[256,64,64]	512
ConvTranspose2d	[128,128,128]	524,416
ReLU	[128,128,128]	0
ConvTranspose2d	[64,256,256]	131,136
ReLU	[64,256,256]	0
Conv2d	[3,256,256]	9,411
Sigmoid	[3,256,256]	0

Table 2. The network architecture of our generator.